Accurate measurement of heteronuclear dipolar couplings by phase-alternating R-symmetry (PARS) sequences in magic angle spinning NMR spectroscopy

Guangjin Hou,[a),b)] Xingyu Lu,[b),c)] Alexander J. Vega,[c)] and Tatyana Polenova[a)]
Department of Chemistry and Biochemistry, University of Delaware, Newark, Delaware 19716, USA and Pittsburgh Center for HIV Protein Interactions, University of Pittsburgh School of Medicine, 1051 Biomedical Science Tower 3, 3501 Fifth Ave., Pittsburgh, Pennsylvania 15261, USA

(Received 22 May 2014; accepted 18 August 2014; published online 11 September 2014)

We report a Phase-Alternating R-Symmetry (PARS) dipolar recoupling scheme for accurate measurement of heteronuclear ^{1}H-X (X = ^{13}C, ^{15}N, ^{31}P, etc.) dipolar couplings in MAS NMR experiments. It is an improvement of conventional C- and R-symmetry type DIPSHIFT experiments where, in addition to the dipolar interaction, the ^{1}H CSA interaction persists and thereby introduces considerable errors in the dipolar measurements. In PARS, phase-shifted RN symmetry pulse blocks applied on the ^{1}H spins combined with π pulses applied on the X spins at the end of each RN block efficiently suppress the effect from ^{1}H chemical shift anisotropy, while keeping the ^{1}H-X dipolar couplings intact. Another advantage over conventional DIPSHIFT experiments, which require the signal to be detected in the form of a reduced-intensity Hahn echo, is that the series of π pulses refocuses the X chemical shift and avoids the necessity of echo formation. PARS permits determination of accurate dipolar couplings in a single experiment; it is suitable for a wide range of MAS conditions including both slow and fast MAS frequencies; and it assures dipolar truncation from the remote protons. The performance of PARS is tested on two model systems, [^{15}N]-*N*-acetyl-valine and [U-^{13}C,^{15}N]-*N*-formyl-Met-Leu-Phe tripeptide. The application of PARS for site-resolved measurement of accurate ^{1}H-^{15}N dipolar couplings in the context of 3D experiments is presented on U-^{13}C,^{15}N-enriched dynein light chain protein LC8. © *2014 AIP Publishing LLC*. [http://dx.doi.org/10.1063/1.4894226]

INTRODUCTION

The measurement of heteronuclear (i.e., ^{1}H-^{15}N and ^{1}H-^{13}C) dipolar couplings is critical as these couplings provide structural and dynamics information in a broad range of systems, such as proteins, biopolymers, and organic solids.[1–11] The knowledge of precise dipolar couplings is important for determination of accurate molecular structures and for quantification of the molecular motions. Even though a variety of pulse schemes have been developed to reintroduce ^{1}H-X dipolar couplings under slow and fast magic-angle spinning (MAS) conditions,[12–26] most of them suffer from insufficient suppression of the strong ^{1}H-^{1}H dipolar couplings and from the RF power limitations imposed on the probes. One approach to reduce the ^{1}H-^{1}H homonuclear dipolar interactions and enable accurate measurements of heteronuclear dipolar couplings involves extensive sample deuteration.[10,21,23] To attain the RF power within the probe specifications, MAS frequencies below 20 kHz are usually used for practical reasons.[12–14,18] Obviously, such approaches preclude measurements in fully or extensively protonated samples and at fast MAS frequencies, effectively limiting the range of systems accessible for analysis to biomolecules of fairly small size.

As reported previously,[15–17,22,27–29] rotor-synchronized RN-symmetry sequences are well suited for the determination of heteronuclear dipolar couplings in fully protonated systems under a wide range of conditions, including fast MAS.[22] They have now become the conventional versions of the original dipolar chemical shift correlation (DIPSHIFT) or separated local field (SLF) schemes.[30–32] We have recently demonstrated that ^{1}H-X (X = ^{13}C, ^{15}N, etc.) dipolar lineshapes recorded using the conventional DIPSHIFT-RN sequences are affected to a non-negligible extent by the chemical shift anisotropy (CSA) interaction of the bonded protons, especially at high magnetic fields.[33,34] While in these experiments recoupling of the ^{1}H-X dipolar interaction is accomplished by RF field irradiations applied on ^{1}H spins, the ^{1}H CSA interaction is thereby also reintroduced. The resulting lineshapes thus contain the contribution of the ^{1}H CSA, reducing the accuracy of the derived ^{1}H-X dipolar couplings at high magnetic fields. One recent approach we introduced in order to overcome this obstacle in accurate measurements of both ^{1}H-X dipolar and ^{1}H CSA parameters is based on performing three independent lineshape experiments to reintroduce (i) mostly ^{1}H-X dipolar interaction; (ii) mostly ^{1}H CSA interaction; and (iii) combined ^{1}H-X dipolar and ^{1}H CSA interactions.[33,34] Simultaneous triple fitting of these three RN line shapes yields accurate ^{1}H CSA and ^{1}H-X dipolar interaction parameters, including the relative orientation

a)Authors to whom correspondence should be addressed. Electronic addresses: hou@udel.edu and tpolenov@udel.edu. Tel.: (302) 831-1968. FAX: (302) 831-6335.
b)G. Hou and X. Lu contributed equally to this work.
c)Electronic addresses: luxingyu@udel.edu and lexvega@comcast.net

between two tensors. The obvious drawbacks of this protocol are that (i) three multi-dimensional, usually time-consuming experiments are required to be performed, and (ii) the data analysis is labor intensive, particularly if one is only interested in the ^{1}H-X heteronuclear dipolar interactions.

Herein, we present a modified RN-symmetry based method that recouples the ^{1}H-X heteronuclear dipolar interactions while suppressing efficiently the ^{1}H CSA interactions. It permits accurate measurement of ^{1}H-X heteronuclear dipolar couplings in a single experiment. The approach is based on the fact that the values of the ^{1}H-X dipolar and ^{1}H CSA interactions recoupled by RN-type symmetry pulse sequences, such as $R18_1^7$, $R12_1^4$, $R14_2^3$, $R20_3^4$, obtain opposite signs when the RF-pulse phases are shifted by 180°. By alternate phase shifting of subsequent RN pulse cycles, both the ^{1}H-X dipolar and the ^{1}H CSA interactions are therefore suppressed. To selectively restore the ^{1}H-X dipolar couplings, additional π pulses are applied on the X spin at the ends of all RN blocks. We refer to this method as a phase-alternating R-type symmetry (PARS) pulse sequence. The PARS dipolar recoupling sequence also results in nearly complete suppression of ^{1}H-^{1}H homonuclear dipolar couplings; it is suitable for a wide range of MAS conditions including both slow and fast MAS frequencies; and it assures dipolar truncation from the remote protons. Theoretical treatment in conjunction with the analysis of the experimental parameters indicates that accurate ^{1}H-X dipolar parameters are yielded by the PARS method. Experimental performance is tested on [^{15}N]-*N*-acetyl-valine (NAV) and [U-^{13}C,^{15}N]-*N*-formyl-Met-Leu-Phe tripeptide (MLF), at MAS frequencies of 20 and 40 kHz. The accuracy of ^{1}H-X heteronuclear dipolar measurements and the effects of RF field inhomogeneity and RF field mismatch are discussed. An application of this method is presented for U-^{13}C,^{15}N-enriched dynein light chain protein (LC8). This approach as implemented in 2D and 3D experiments is generally suited for recording accurate ^{1}H-X heteronuclear dipolar couplings in a variety of systems, including proteins and protein assemblies as well as other inorganic, organic, and biological solids.

EXPERIMENTS AND METHODS

Materials

U-^{15}N-labeled *N*-acetyl-valine (NAV) and U-^{13}C,^{15}N-labeled *N*-formyl-Met-Leu-Phe (MLF) tripeptide were purchased from Cambridge Isotope Laboratories and used without further purification or re-crystallization. Both powder samples were packed into 1.6 mm Varian MAS rotors for subsequent NMR experiments. U-^{13}C,^{15}N dynein light chain (LC8) protein was expressed in *Escherichia coli* and purified as described previously.[35] The solid-state sample was generated by controlled precipitation through slow addition of 30% polyethylene glycol (PEG)-3350 to the solution of LC8 protein. The protein was doped with 5 mM Cu(II)-EDTA prior to the precipitation step, and the precipitated protein sample was packed into a 1.9 mm Bruker rotor for subsequent NMR experiments.

NMR spectroscopy

All NMR experiments were applied to ^{1}H-^{15}N spin pairs and recorded at 14.1 T on a Varian InfinityPlus or at 19.97 T on a Bruker AVIII NMR spectrometer, operating at Larmor frequencies of 599.8/850.4 MHz for ^{1}H, 150.8/213.8 MHz for ^{13}C, and 60.8/86.2 MHz for ^{15}N, respectively. For the 14.1 T experiments, a Varian 1.6 mm MAS triple-resonance HXY probe was used. The MAS frequency was 20 or 40 kHz, and controlled to within ±5 Hz by the Varian MAS controller. The typical 90° pulse lengths were 1.4 μs (^{1}H), 2.5 μs (^{13}C), and 3.5 μs (^{15}N). For the 19.9 T experiments, a Bruker 1.9 mm MAS triple-resonance probe was used. The MAS frequency was 20 kHz, and controlled to within ±2 Hz by the Bruker MAS controller. The typical 90° pulse lengths were 2.05 μs (^{1}H), 2.8 μs (^{13}C), and 3.2 μs (^{15}N). To reduce sample heating during MAS, nitrogen gas was used for cooling, resulting in a final sample temperature of 20 °C for NAV and MLF samples and 0 °C for LC8 protein.

In addition to the PARS experiments, the triple-experiment approach, previously established by us for the accurate ^{1}H CSA and ^{1}H-^{15}N dipolar measurements,[33,34] was also applied, in order to compare the accuracy of the ^{1}H-^{15}N dipolar coupling parameters determined by various recoupling sequences. These three experiments are the conventional DIPSHIFT-RN or RN-X pulse sequence shown in Figure 1(a) and the RN-^{1}H(X_{dec}) and RN-^{1}H(X_{und}) sequences shown in Figure 1(b). The X_{dec} version has decoupling π pulses on the *S* channel at the centers of the RN_0 cycles, and they are switched off in the X_{und} version. The RN_0 blocks represent suitable RN_n^ν sequences, such as $R12_1^4$, $R14_2^3$, $R18_1^7$, $R18_2^5$, $R20_3^4$, consisting of a windowless series of N π pulses covering n rotor cycles with RF amplitude $(N/2n)\omega_R$ and alternating phases $\pm(\nu/N)\pi$.[27–29] Figure 1(c) shows the 2D version of the PARS sequence applied to NAV and MLF. In PARS experiments, the RN cycles alternate between RN_0, having the same pulse phase as in Figures 1(a) and 1(b), and RN_π, having its phases shifted by 180°. The PARS spectrum of LC8 was obtained with the 3D experiment shown in Figure 1(e). A real acquisition mode is used for the t_1 dipolar evolution periods in all PARS and RN NMR experiments.

For the 2D PARS experiments (Figure 1(c)) as well as conventional DIPSHIFT-RN experiments (Figure 1(a)) on NAV and MLF at 14.1 T, the ^{1}H-^{15}N cross polarization was performed with a linear amplitude ramp (80%–100%) on the ^{15}N channel, the RF field of the ramp center being 50 kHz, with the optimized RF field on the ^{1}H channel Hartmann-Hahn matched to the high-frequency first spinning sideband. The contact time was 1.3 ms and the recycle delay was 3.0 s. For the ^{1}H-^{15}N dipolar experiments conducted at the MAS frequency of 20 kHz, ^{1}H RF field strengths were 90 kHz for $R18_2^5$, 120 kHz for $R12_1^4$, 140 kHz for $R14_1^5$, and 180 kHz for $R18_1^7$ symmetry pulses. For ^{1}H-^{15}N dipolar experiments performed at the MAS frequency of 40 kHz, ^{1}H RF field strengths were 133.3 kHz for $R20_3^4$, 140 kHz for $R14_2^3$, and 180 kHz for $R18_2^5$ symmetry pulses. Each RF field strength $(N/2n \cdot \omega_R)$ was optimized directly on the sample under study by adjusting it to obtain a vanishing CP-detected ^{15}N

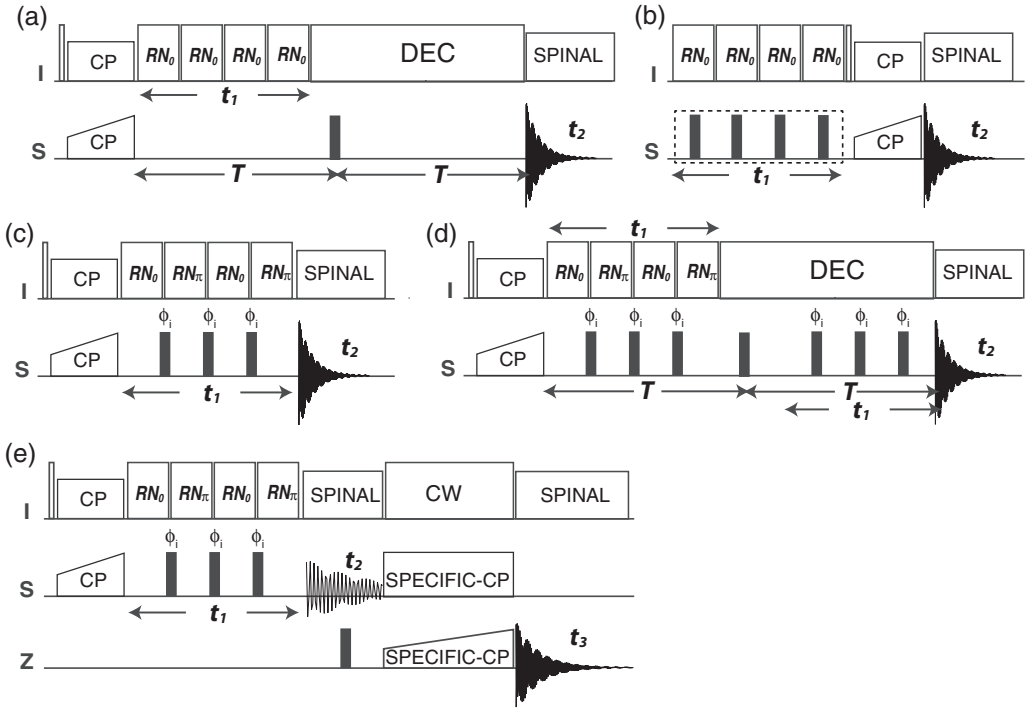

FIG. 1. Pulse sequences applied to ^{1}H-X (*I*-*S*) spin pairs for 2D (a) conventional RN-based DIPSHIFT, (b) proton CSA recoupling with decoupling or undecoupling of *I*-*S* dipolar interactions, RN-^{1}H(X_{dec}) or RN-^{1}H(X_{und}),[33,34] (c) regular PARS, (d) constant-time PARS, and (e) 3D PARS heteronuclear dipolar measurements. Blank and solid squares denote $\pi/2$ and π pulses, respectively. During PARS t_1 period, the symmetry block RN_0 and its π-phase-shifted symmetry pulse block RN_π are applied on *I* spin alternately, while the series of π pulses are applied to *S* spin at the end of each RN block. In (e), SPECIFIC-CP is used to establish NCA or NCO chemical shift correlations.

signal following a ^{1}H pulse having the required π pulse length ($\nu\tau_R/N$). For PARS experiments, a π pulse with pulse length of 7 μs was applied on the ^{15}N spin at the end of each RN block. The sequence of π pulses is applied with a 2-, 4-, or 8-step phase cycle, having phases $(x, -x)$, $(x, -x, -x, x)$, or $(x, -x, -x, x, -x, x, x, -x)$, respectively.

The triple-RN experiments shown in Figures 1(a) and 1(b) employed the $R18_1^7$ based recoupling at a MAS frequency of 20 kHz. For the R18-^{1}H($^{15}N_{dec}$) and R18-^{1}H($^{15}N_{und}$) experiments (Figure 1(b)), the ^{1}H-^{15}N CP contact time was set to two rotor periods, 100 μs. For R18-^{1}H($^{15}N_{dec}$), 7.0 μs-wide π pulses were applied on ^{15}N at the centers of the RN cycle. All other experimental parameters of these three experiments were the same as for the R18-PARS measurement.

For the 19.9 T experiments on U-^{13}C,^{15}N-LC8 protein, a 3D $R12_1^4$-based PARS sequence (Figure 1(e)) and a conventional DIPSHIFT-R12 sequence were used for recording ^{1}H-^{15}N dipolar couplings. The MAS frequency was 20 kHz. A π pulse (pulse length was 6.4 μs) was applied on the ^{15}N spin at the end of each RN block. The band-selective magnetization transfer from ^{15}N to $^{13}C\alpha$ was realized by SPECIFIC-CP with tangent amplitude ramp on the ^{13}C spin with center amplitude at 50 kHz, and the optimized ^{15}N-^{13}C DCP contact time was 4.5 ms. SPINAL-64[36] ^{1}H decoupling with RF field of 120 kHz was used during t_2 and t_3 periods, and CW ^{1}H decoupling with RF field of 125 kHz was employed for SPECIFIC-CP period. A total of 16 t_1 and 48 t_2 increments were used to record both 3D PARS-R12 and conventional DIPSHIFT-R12 spectra, and 128 scans with a pulse delay of 2.0 s were accumulated for each increment.

NMR numerical simulations

All numerical simulations were performed using the SIMPSON software[37] and/or a home written Fortran-95 program.[33] 320 REPULSION[38] angles (α, β) were used to generate a powder average for all R-type and C-type symmetry-based sequences. For R- and C-type sequences, we summed over 5 and 64 γ angles, respectively. To extract the best-fit ^{1}H-^{15}N dipolar coupling constants, the NMR parameters used in the simulations were the same as in the corresponding experiments. For all PARS and DIPSHIFT ^{1}H-X dipolar measurements, single fitting was performed using the Minuit package in the SIMPSON program. The home written Fortran-95 program was used for triply fitting RN-^{1}H($^{15}N_{dec}$), RN-^{1}H($^{15}N_{und}$), and RN-^{15}N spectra to extract ^{1}H CSA, ^{1}H-^{15}N dipolar and also the relative tensor orientation parameters.

RESULTS AND DISCUSSION

General properties of PARS sequences: Theory and numerical simulations

Nuclear spin interactions can be conveniently classified into various symmetry groups according to their spatial rank *l* and their spin rank λ, and these symmetry properties can in

turn be exploited in the design of MAS experiments for recoupling of the desired spin interactions.[27–29] According to this framework, the CSA and heteronuclear dipolar interactions have the same symmetry properties, $l = 2$ and $\lambda = 1$, which means that rotor-synchronized pulse sequences with appropriate symmetry features would simultaneously decouple or recouple both CSA and heteronuclear dipolar interactions under MAS.[39] Most of ^{1}H-X (X = ^{13}C, ^{15}N, etc.) dipolar recoupling techniques require rotor-synchronized RF field irradiation to be applied on the ^{1}H spin, and the magnetization of X spins then evolves under the modulation of the reintroduced ^{1}H-X heteronuclear dipolar interactions. Even though some of these heteronuclear dipolar recoupling sequences can suppress efficiently the strong ^{1}H-^{1}H homonuclear dipolar couplings, ^{1}H CSA interactions would be recoupled together with the heteronuclear dipolar couplings during the application of rotor-synchronized RF pulses on protons, in turn affecting the dipolar-modulated evolution of X spins to a greater or lesser degree.[33,34]

Due to the above, ^{1}H CSA generally introduces some inaccuracy in the measurement of the dipolar interaction parameters, particularly of ^{1}H-^{15}N amide group couplings in proteins, and especially at high magnetic fields. One approach that we have recently established for accurate measurements of both heteronuclear dipolar couplings and ^{1}H CSAs under such conditions requires three independent multidimensional lineshape experiments to reintroduce (i) mostly HX dipolar couplings; (ii) mostly ^{1}H CSA interaction; and (iii) combined HX dipolar and ^{1}H CSA interaction.[33,34] These experiments, schematically depicted in Figures 1(a) and 1(b), are designed to (i) record the evolution of the X magnetization during RN irradiation, (ii) record the evolution of the ^{1}H-magnetization during RN irradiation while decoupling X, and (iii) record ^{1}H magnetization while leaving X undecoupled. We refer to these experiments as (i) RN-X, (ii) RN-^{1}H(X_{dec}), and (iii) RN-^{1}H(X_{und}), respectively.[33,34] RN_n^{ν} sequences that are suitable for these experiments satisfy the relation $N = 4n + 2\nu$, [27–29] such as $R12_1^4$, $R14_2^3$, $R18_1^7$, $R18_2^5$, and $R20_3^4$.

Averaged to first order over such an RN cycle, the Hamiltonian of a single axially-symmetric *I*-*S* heteronuclear dipolar interaction ($I = ^1$H, $S = $ X) is given by

$$H_{av}^{D} = -\kappa_{2211} D \sin^2 \beta_D (I_x S_z \cos 2\gamma_D + I_y S_z \sin 2\gamma_D), \tag{1}$$

where κ_{2211} is a scaling factor that depends on the N,n,ν combination and D is the dipolar coupling constant (DCC), in the absence of motion given by $D = -\mu_0 \gamma_I \gamma_S \hbar / 2r^3$, with r being the internuclear distance. β_D is the angle between the rotor axis and the internuclear *IS* vector and γ_D represents the rotation angle of the *IS* vector at time $t = 0$.[33,34]

The first-order average RN Hamiltonian of a CSA tensor of *I*, its principal coordinates δ_{xx}, δ_{yy}, δ_{zz} being represented by $\delta_\sigma = \delta_{zz} - \delta_{iso}$, and $\eta = (\delta_{yy} - \delta_{xx})/\delta_\sigma$, is given by

$$\begin{aligned} H_{av}^{CSA} = {} & \tfrac{1}{6}\kappa_{2211}\omega_0\delta_\sigma[\{-3\sin^2\beta_{CSA} + \eta(\cos^2\beta_{CSA} + 1)\cos 2\alpha_{CSA}\}(I_x \cos 2\gamma_{CSA} + I_y \sin 2\gamma_{CSA}) \\ & + 2\eta \cos\beta_{CSA} \sin 2\alpha_{CSA}(I_x \sin 2\gamma_{CSA} - I_y \cos 2\gamma_{CSA})], \end{aligned} \tag{2}$$

where ω_0 is the Larmor frequency, α_{CSA} and β_{CSA} are the azimuthal and polar angles of the rotor axis with respect to the CSA principal axes, and γ_{CSA} represents the rotation angle of the CSA tensor at $t = 0$.[33,34] To first order, the RN-X and RN-^{1}H(X_{und}) spectra are both determined by the combined I_xS_z, I_yS_z, I_x, and I_y terms of H_{av}^D and H_{av}^{CSA}, while RN-^{1}H(X_{dec}) depends only on H_{av}^{CSA}. In higher-order effective Hamiltonians the coefficients of these terms are slightly adjusted, and additional terms with spin operators I_z and I_zS_z are also introduced. Powder spectra thus depend on the parameters D, and the polar and azimuthal angles β and α of the vector with respect to the principal axes of the CSA tensor.

Examples of the effect of ^{1}H CSA on simulated spectra of the conventional DIPSHIFT RN-X experiment are shown in Figure 2 and in Figure S1 in the supplementary material.[49] To show that similar complications arise in C-symmetry-based DIPSHIFT experiments, examples of such simulated dipolar spectra are also included. We have used an HN-spin-pair system described by an axially symmetric ^{1}H-^{15}N dipolar interaction of 10 kHz and incorporated various ^{1}H CSA parameters to assess their effect on the dipolar lineshapes recoupled by the sequences: $R12_1^4$ and $C5_1^1$ (TMREV[14]). Both DIPSHIFT-R12 and TMREV-C5 sequences can efficiently reintroduce the MAS-averaged ^{1}H-^{15}N dipolar interactions, as shown in the dipolar powder patterns. It is clear from the figure that the recoupled ^{1}H CSA and ^{1}H-^{15}N dipolar interactions interfere with each other during the symmetry pulses applied to the protons, resulting in lineshapes possessing complex fine structure. As seen in Figures 2(a) and 2(b), both the dipolar splitting and the fine structure of the lineshapes are affected by the ^{1}H CSA interaction, and the distortion of the dipolar lineshapes becomes more severe as the ^{1}H δ_σ increases or when the CSA z axis is not collinear with the H-N bond. We also note that the magnitude of the distortions is field dependent; the higher the field, the more prominent the effect of ^{1}H CSA on dipolar lineshapes becomes. As shown in Figure S1 in the supplementary material,[49] the simulated ^{1}H-^{15}N DIPSHIFT-R12 and TMREV-C5 dipolar lineshapes are increasingly distorted when the ^{1}H Larmor frequency is raised from 400 to 1000 MHz. To get an impression of the impact that this effect can have on DCC determination, we chose the 800 MHz DIPSHIFT-$R12_1^4$ spectrum shown in Figure S1

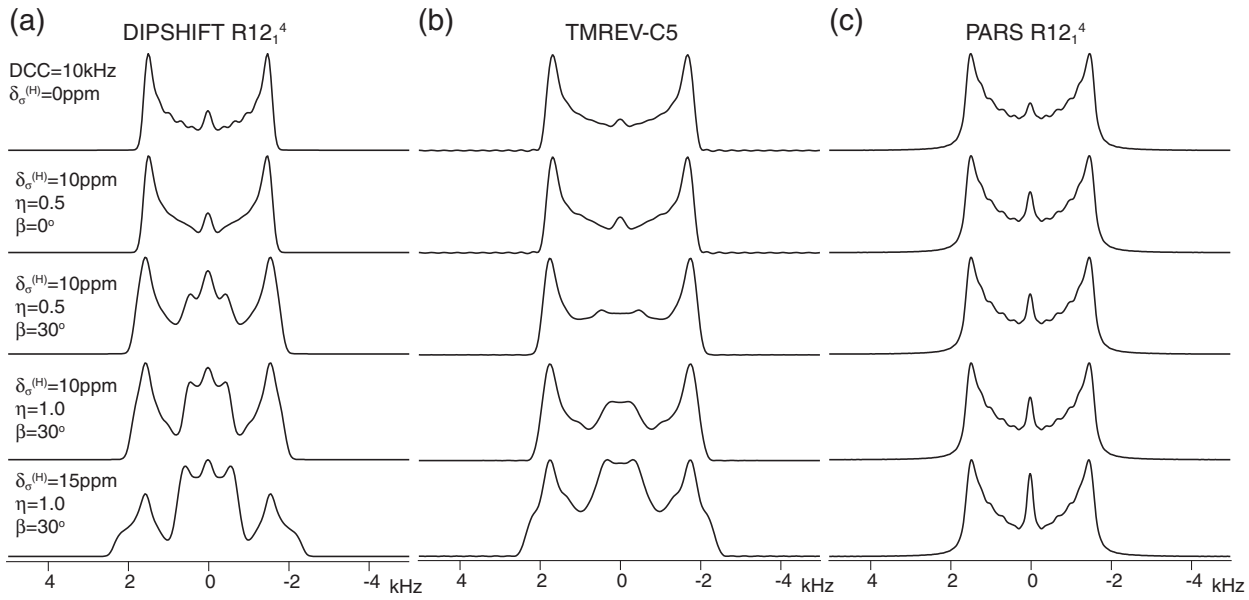

FIG. 2. Simulated ^{1}H-^{15}N dipolar line shapes recoupled by the (a) R12$_1^4$-based regular DIPSHIFT, (b) C-type TMREV-5, and (c) R12$_1^4$-based PARS sequences at magnetic field of 14.1 T (^{1}H Larmor frequency of 600 MHz), with dipolar coupling constant (DCC) of 10 kHz and various ^{1}H CSA parameters. The MAS frequency is 20 kHz for DIPSHIFT and PARS, and 10 kHz for TMREV-5. The ^{1}H RF field strength is 120 kHz for DIPSHIFT and PARS recoupling sequences, and 150 kHz for TMREV-5.

in the supplementary material,[49] which was simulated with a DCC of 10 kHz and a ^{1}H CSA of 10 ppm, and fitted it under the assumption that the CSA vanishes. It gave a best-fit DCC of 11.3 kHz. The same procedure at 600 MHz led to 10.7 kHz.

The motivation for the current study is to establish a recoupling method that can provide efficient averaging of the ^{1}H CSA in the context of efficient recoupling of heteronuclear dipolar interaction. Our approach takes advantage of the phases of the RF pulses that make up an RN sequence. A standard RN_n^ν pulse cycle consists of N single π pulses whose RF phases alternate between $\pi\nu/N$ and $-\pi\nu/N$. If those phases are shifted by 180° to $(\pi\nu/N + \pi)$ and to $(-\pi\nu/N + \pi)$, then the average Hamiltonians of Equations (1) and (2) remain the same, except that the signs of the coefficients are inverted. Numerical evaluations have shown that even in effective Hamiltonians that include higher-order corrections, a 180° phase shift causes the coefficients of the I_xS_z, I_yS_z, I_x, and I_y terms to change their signs without changing their magnitude. As a result the average Hamiltonian of a double cycle, consisting of a standard RN$_0$ cycle and a phase-shifted RN$_\pi$ cycle, vanishes, leading to suppression of both ^{1}HX dipolar and ^{1}H CSA interactions. If, in addition, π pulses are applied on the S spin in the middle and at the end of each combined (RN$_0$ RN$_\pi$) symmetry block, the inverting operation on the S spins restores the original signs of the I_xS_z and I_yS_z coefficients while leaving the I_x and I_y terms in sign-alternating mode. As a result, this Phase-Alternating R-type Symmetry (PARS) pulse sequence keeps the *I-S* dipolar interactions intact while it suppresses the CSA interactions of spin I. As will be shown below, this PARS approach satisfactorily meets our goal of measuring ^{1}H-X DCCs without interference of ^{1}H CSA interactions. It must be added that while a 180° phase shift of the RN cycle inverts the signs of the most relevant terms of the average Hamiltonian, the higher-order corrections of the types I_z and I_zS_z remain unaffected by the phase shift. Of those, I_zS_z is canceled by the π pulses but I_z is not, leading to some effect on the lineshapes to be discussed below and in the supplementary material.[49]

A straightforward implementation of the PARS approach is shown in Figure 1(c). It differs from the conventional RN-X experiment shown in Figure 1(a) not only by the phase alternations of RN blocks and the π pulses on the S channel but also by the omission of an additional spin-echo formation needed to enable refocused signal detection in RN-X. It can obviously be avoided because the π pulse sequence already refocuses the S chemical shifts. In the case of ^{1}H-^{15}N PARS dipolar experiments, the interactions with nearby ^{13}C nuclei are also to be considered. While MAS and the series of π pulses effectively decouple their interaction with ^{15}N, they do have a minor effect on conventional DIPSHIFT-RN spectra because the ^{1}H-^{13}C dipolar interaction is experienced by the ^{1}H nuclei as similar to their CSA. However, in PARS it is suppressed, such that ^{13}C decoupling is not necessary, further distinguishing it from conventional DIPSHIFT-RN.

The recoupled *I-S* dipolar evolution is modulated by the T_2 decay of the S spin during t_1 period, which causes additional line broadening in the *I-S* PARS dipolar spectrum. Usually the decay rate of the T_2 relaxation is much slower than the size of the *I-S* dipolar couplings (which are of the order of 10 kHz). Therefore, in practice the T_2 decay of S spin does not affect the accuracy of the PARS dipolar measurements and is simply represented by the empirical line broadening parameter used during the fitting of the PARS dipolar line shape. To suppress the additional T_2 decay of the *I-S* dipolar evolution during the t_1 period, constant-time (CT) PARS sequence can be employed (Figure 1(d)), which leads to enhanced resolution of the *I-S* PARS dipolar spectrum, provided the T_2 decay rate during PARS irradiation is not much faster

than that during ^{1}H decoupling. This experiment is particularly well suited for the accurate determination of weak dipolar couplings and in systems with short T_2 relaxation times. However, the constant-time spin echo brings sensitivity loss due to the constant T_2 decay, which might result in the disappearance of the resonances with very limited sensitivities. As mentioned above, the spin-echo formation cannot be avoided in conventional DIPSHIFT-RN experiments. For the applications in large or complicated systems, an extra isotropic chemical shift dimension is required to attain the necessary site resolution, and the 3D implementation of PARS-based dipolar recoupling is illustrated in Figure 1(e), where an additional heteronuclear magnetization transfer to Z is introduced through SPECIFIC-CP.[40]

Figure 2(c) shows simulated ^{1}H-^{15}N PARS spectra. To reflect practical experimental conditions, the π pulses on the S channel were given finite lengths centered at the joints of the RN_0 and RN_π cycles. Contrary to the behavior observed in Figures 2(a) and 2(b) for the conventional R- and C-symmetry based dipolar recoupling, the PARS recoupling can be seen to refocus efficiently the ^{1}H CSA interactions and to give rise to essentially pure ^{1}H-X dipolar powder patterns. With $R12_1^4$-based PARS sequence, ^{1}H-^{15}N dipolar lineshape is not affected to any significant extent by the presence of ^{1}H CSA except that a slight increase in the central peak intensity is observed, due to the contributions from partially unrefocused higher-order Hamiltonian terms, notably the I_z term mentioned above. It is clear that the PARS dipolar splittings and lineshape features (except for the central peak intensity) are not affected at all by the ^{1}H CSA interaction, permitting accurate measurement of ^{1}H-X dipolar parameters from a single PARS spectrum. Furthermore, the PARS dipolar line shapes are independent of the magnetic field, as shown in Figure S1 in the supplementary material.[49] Due to the complete suppression of ^{1}H CSA interactions, the PARS dipolar lineshapes are in principle able to yield not only the dipolar coupling constant (DCC) but also the dipolar asymmetry parameter (η_D), the latter directly reporting on the presence and symmetry of motions occurring on timescales matching the magnitude of the dipolar interaction. In this work, we limit the discussion to axially symmetric ^{1}H-X dipolar interactions and note that the presence of dipolar asymmetry does not change any of the conclusions but requires taking into account the rhombicity of the dipolar tensor in numerical simulations.

Experimental evidence of the reliability of PARS sequences

To experimentally verify our prediction that accurate dipolar measurements can be extracted from a single PARS spectrum, the above-mentioned series of three experiments that we originally developed for simultaneous ^{1}H CSA and ^{1}H-X DCC measurements[33] can be performed. For this purpose, the three $R18_1^7$-^{1}H($^{15}N_{und}$), $R18_1^7$-^{1}H($^{15}N_{dec}$), and $R18_1^7$-^{15}N 2D spectra were recorded on ^{15}N labeled NAV. The corresponding experimental and simulated line shapes are shown in Figure 3(a). For extracting accurate ^{1}H CSA and ^{1}H-^{15}N dipolar interactions, as well as the relative tensor orientations, we have performed a simultaneous triple fit of the experimental line shapes according to the protocol reported previously. The best-fit parameters are listed in Table I. The ^{1}H-^{15}N dipolar coupling constant measured according to this

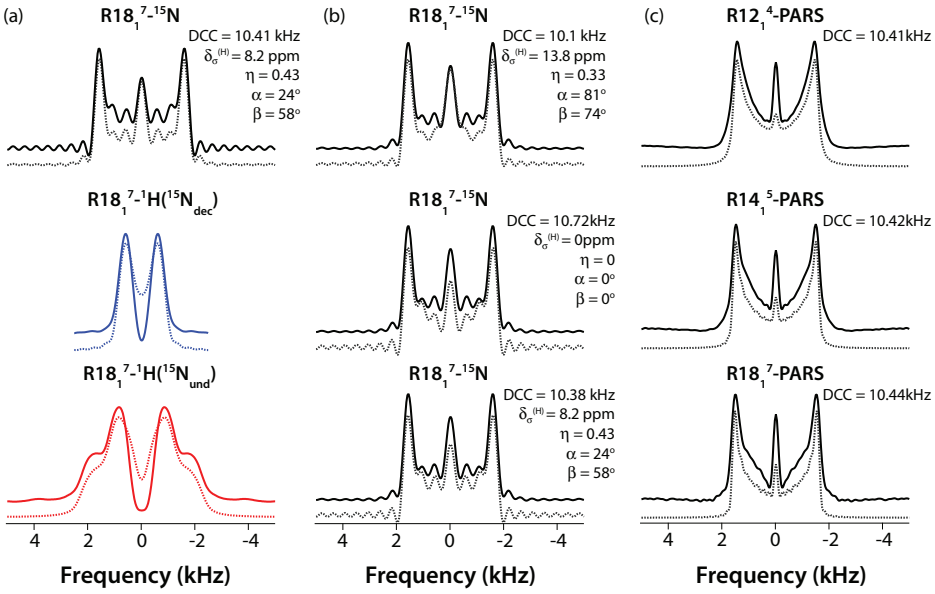

FIG. 3. Experimental (solid lines) and best-fit (dotted lines) RN spectra of [^{15}N]-*N*-acetyl valine (NAV), recorded at the magnetic field of 14.1 T and MAS frequency of 20 kHz. (a) RN-^{1}H($^{15}N_{und}$) (red), RN-^{1}H($^{15}N_{dec}$) (blue), and RN-^{15}N (black) line shapes obtained by $R18_1^7$ symmetry sequences. The best-fit ^{1}H-^{15}N dipolar, ^{1}H CSA, and relative orientation parameters were obtained by simultaneous triple fit of the spectra. (b) ^{1}H-^{15}N dipolar line shape obtained by DIPSHIFT-$R18_1^7$ recoupling sequence. The spectrum was fitted to extract the dipolar coupling constant, using different fixed values of ^{1}H CSA parameters, shown next to each spectrum. Note the different resulting DCC values depending on the ^{1}H CSA used. (c) Single-fitted ^{1}H-^{15}N dipolar line shapes obtained by PARS with various RN symmetry sequences, $R12_1^4$ with ^{1}H RF field of 120 kHz (top), $R14_1^5$ with ^{1}H RF field of 140 kHz (middle), and $R18_1^7$ with ^{1}H RF field of 180 kHz (bottom). The ^{15}N π pulses during PARS period were 7.0 μs wide and were applied with 8-step phase cycle.

TABLE I. NMR experimental ^{1}H-^{15}N dipolar coupling parameters of [^{15}N]-*N*-acetyl-valine (NAV) and [^{13}C,^{15}N]-N-formyl-Met-Leu-Phe (MLF) by various recoupling techniques, recorded at MAS frequency of 20 kHz.

Sample	Method	δ_σ ^{H}	η	α[a]	β[a]	H-N DCC
NAV	Tri-RN	8.2	0.43	24°	58°	10.41 kHz
	DIPSHIFT-R18	13.8[b]	0.33[b]	81°[b]	74°[b]	10.10 kHz
	DIPSHIFT-R18	0[b]	0[b]	0°[b]	0°[b]	10.72 kHz
	DIPSHIFT-R18	8.2[c]	0.43[c]	24°[c]	58°[c]	10.38 kHz
	PARS-R12	…	…	…	…	10.41 kHz
	PARS-R14	…	…	…	…	10.42 kHz
	PARS-R18	…	…	…	…	10.44 kHz
MLF-Met	PARS-R12	…	…	…	…	10.33 kHz
	PARS-R14	…	…	…	…	10.38 kHz
	PARS-R18	…	…	…	…	10.34 kHz
MLF-Leu	PARS-R12	…	…	…	…	10.23 kHz
	PARS-R14	…	…	…	…	10.25 kHz
	PARS-R18	…	…	…	…	10.18 kHz
MLF-Phe	PARS-R12	…	…	…	…	10.36 kHz
	PARS-R14	…	…	…	…	10.40 kHz
	PARS-R18	…	…	…	…	10.37 kHz

[a]α and β are the polar angles of the NH bond direction with respect to the ^{1}H CSA principal axis system.
[b]These parameters were kept fixed.
[c]H CSA parameters were fixed at the best-fit values extracted from the triple fits of the ^{1}H CSA data.

procedure is 10.41 kHz. To assess the errors in the dipolar couplings when they are determined by a single fit of a conventional DIPSHIFT recorded line shape, we have used the RN-^{15}N spectrum of ^{15}N-NAV. If correct ^{1}H CSA parameters are used, the best-fitted ^{1}H-^{15}N DCC, extracted from a single spectrum, is 10.38 kHz, consistent with the value obtained from the triple fit (Figure 3(b)). However, the ^{1}H CSA parameters are not known *a priori* and exhibit variability for amide protons in proteins, as we and others have demonstrated previously.[33,41–44] As illustrated in Figure 3(b) and Table I, setting ^{1}H CSA parameters to different values results in pronounced variation of the ^{1}H-^{15}N dipolar coupling constant extracted from the data: the apparent DCC varies between 10.10 and 10.72 kHz when ^{1}H δ_σ is set between 13.8 and 0 ppm. (We note that in CAP-Gly protein, we observed ^{1}H δ_σ to range from 4.6 to ca. 10.6 ppm[33] and in histidine to 17.4 ppm.[34])

On the contrary, the measurement of accurate ^{1}H-^{15}N dipolar coupling constant in PARS experiments does not require any knowledge of the ^{1}H CSA. ^{1}H-^{15}N PARS dipolar spectra acquired on NAV with different RN symmetry pulses are shown in Figure 3(c). The best-fit ^{1}H-^{15}N DCCs are 10.41 kHz (for $R12_1^4$ PARS), 10.42 kHz (for $R14_1^5$ PARS), and 10.44 kHz (for $R18_1^7$ PARS), all in excellent agreement with the DCC value of 10.41 kHz extracted from the triple fit of the RN-^{1}H(^{15}N$_{und}$), RN-^{1}H(^{15}N$_{dec}$), and RN-^{15}N spectra. This experimental result corroborates our predictions borne out of theoretical considerations and numerical simulations. We also note that any suitable-symmetry R-sequences can be used in PARS sequences, permitting the experimentalist to fine-tune the conditions to the available hardware.

We also examined the performance of the $R12_1^4$-, $R14_1^5$-, and $R18_1^7$-based PARS sequences for ^{1}H-^{15}N dipolar measurements on U-^{13}C,^{15}N labeled MLF tripeptide. Figure 4 shows the experimental ^{1}H-^{15}N dipolar line shapes extracted from 2D PARS NMR spectra together with the best-fit line shapes (using full Hamiltonian) for each MLF residue. As summarized in Table I, the best-fit ^{1}H-^{15}N DCCs extracted from the individual measurements are in excellent agreement, and display very small variations between the three experiments. The average values for each residue are 10.35 ± 0.03 kHz for Met, 10.22 ± 0.04 kHz for Leu, and 10.38 ± 0.02 kHz for Phe, illustrating the robustness of PARS.

Sensitivity of PARS sequences to RF field mismatch

Most of the decoupling and recoupling sequences are sensitive to the RF field mismatch and inhomogeneity to greater or lesser extent. Compared to the conventional DIPSHIFT-RN sequences, PARS requires an additional series of π pulses on the *S* channel to restore the refocused *I*-*S* dipolar couplings, so PARS sequences may be additionally affected by any RF field imperfections on the *S* spin. A deviation of such *x* pulses from π flip angle will not only make the restoration of the ^{1}H-X dipolar interaction incomplete but it will also add an unwanted S_x term to the average Hamiltonian, thereby heavily distorting the *S*-detected spectrum (data not shown). To eliminate the effect of RF field mismatch on the ^{15}N π pulses applied during the PARS period, an appropriate phase cycling is required. We have assessed the sensitivity to the RF field mismatch by recording PARS ^{1}H-^{15}N dipolar spectra in NAV using 2-step (*x*, -*x*), 4-step (*x*, -*x*, -*x*, *x*) and 8-step (*x*, -*x*, -*x*, *x*, -*x*, *x*, *x*, -*x*) phase cycles on the ^{15}N channel. As seen in Figure S2 of the supplementary material,[49] the 2-step phase cycle is insufficient for suppressing the sensitivity to the RF field mismatch, and the dipolar line shapes exhibit distortions, which become more severe as the RF field mismatch is increased. On the contrary, 4- and 8-step phase cycles efficiently suppress sensitivity to the RF field mismatches, and the dipolar line shapes are largely invariant with mismatch, even when the offset of ^{15}N π pulses is as high as ±20°, as can be seen in Figures S2 and S3 in the supplementary material.[49]

Similar to the conventional DIPSHIFT-RN sequences, precise setting of the ^{1}H RF field in the RN symmetry pulses is critical for PARS measurements. As shown in Figure S4 in the supplementary material,[49] PARS sequences are slightly less sensitive to ^{1}H RF field mismatches as compared to the conventional DIPSHIFT-RN sequences. Nevertheless, this effect cannot be neglected, particularly at field mismatches greater than 5 kHz. In general, as we have reported previously, R-symmetry sequences with the ratio of $N/2n > 2.5$ are preferable due to their lower sensitivity to RF field inhomogeneity and mismatch.[22] Some features of the mismatch dependence, including the increased intensity of zero-frequency peaks, are described and explained in the supplementary material.[49] One of the conclusions of that investigation is that in the case of 20% RF inhomogeneity across the sample space (closely representing the actual RF profile of the 1.6 mm NMR probe used in this project), the re-

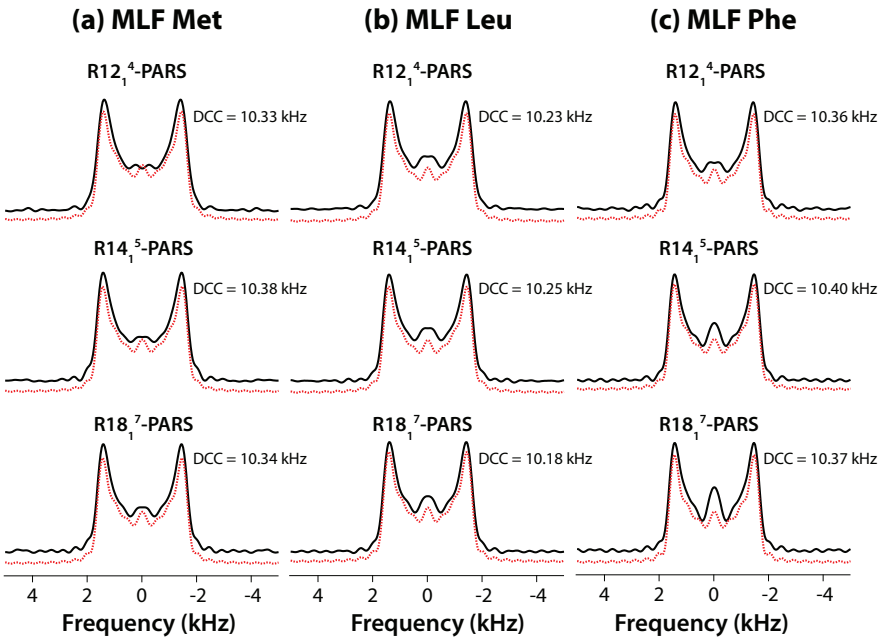

FIG. 4. Experimental (black lines) and simulated (red dashed lines) ^{1}H-^{15}N dipolar line shapes recorded by PARS sequences for residues Met (a), Leu (b), and Phe (c) of [U-^{13}C,^{15}N]-*N*-formyl-Met-Leu-Phe tripeptide. The experiments were conducted at 14.1 T and MAS frequency of 20 kHz. The RF field strength was 120 kHz (R12$_1^4$ PARS, top), 140 kHz (R14$_1^5$ PARS, middle), and 180 kHz (R18$_1^7$ PARS, bottom). The ^{15}N π pulses during PARS period were 7.0 μs wide and were applied with 8-step phase cycle. The best-fit dipolar coupling constants are indicated next to each dipolar lineshape.

sulting apparent DCC is about 3% lower than the actual value. Since this reduction is the same for PARS and DIPSHIFT-RN, we have not applied it to the DCC values determined by fitting of the experimental spectra. Furthermore, the dipolar splittings turn out to slightly depend on the width of the ^{15}N π pulses (not shown). It is therefore important to do the lineshape fittings with the correct pulse width in the simulation protocol.

PARS recoupling under fast MAS

As discussed in our previous report,[22] RN-symmetry sequences are very well suited for ^{1}H-X heteronuclear dipolar measurements under fast MAS conditions (40 kHz and higher). The same applies to PARS sequences. To test the performance of PARS at 40 kHz MAS, we have conducted several PARS experiments on the NAV sample. The resulting ^{1}H-^{15}N PARS dipolar spectra for each PARS sequence are shown in Figure 5(a), together with the corresponding simulated dipolar line shapes. The reduced spectral intensity in the central region is the result of the RF-inhomogeneity-induced central peak, which acquires its intensity by reducing the intensity of dipolar-split signal in its close vicinity, as explained in the supplementary material.[49] This lineshape distortion is more severe at higher MAS frequency because the size of the underlying spin interaction is proportional to it. For this reason, the central regions were excluded from the curve fitting. The best-fit ^{1}H-^{15}N DCCs extracted from these R20$_3^4$-, R14$_2^3$- and R18$_2^5$-based PARS spectra recorded at 40 kHz are in excellent agreement with those extracted at the MAS frequency of 20 kHz. In contrast, the ^{1}H-X heteronuclear dipolar couplings determined by conventional DIPSHIFT at the MAS frequency of 40 kHz are dependent on ^{1}H CSA. As shown in Figure 5(b), the single fits of the ^{1}H-^{15}N conventional R14$_2^3$ spectra depend on the ^{1}H CSA parameters, and the accurate ^{1}H-^{15}N dipolar coupling constant can be extracted only when the correct ^{1}H CSA parameters are used in fitting the spectra.

Application of PARS to biological systems

It is important to know accurate ^{1}H-X dipolar couplings in biological proteins and protein assemblies, since they contain valuable structural and dynamics information. As discussed above, most of the conventional C- or R-symmetry based dipolar recoupling sequences are sensitive to the ^{1}H CSA interactions. ^{1}H CSA depends strongly on molecular environment, including the strength and geometry of hydrogen bonding, which results in considerable variability of ^{1}H CSA parameters in amide protons in proteins.[33,41–46] This variability in turn may obstruct accurate measurements of ^{1}H-X dipolar couplings by conventional sequences, especially at magnetic fields higher than 14 T. The efficient suppression of ^{1}H CSA interactions by the PARS dipolar recoupling sequences (observed even at high fields and for a broad range of MAS conditions including fast MAS) is therefore critical for the accurate measurement of ^{1}H-X dipolar couplings.

To test the performance of PARS for dipolar coupling measurements in fully protonated U-^{13}C,^{15}N-proteins, we have recorded site-specifically ^{1}H-^{15}N dipolar couplings in U-^{13}C,^{15}N dynein light chain (LC8) protein at 19.9 T, using the R12$_1^4$-based 3D PARS sequence shown in Figure 1(e). We have also recorded the corresponding conventional R12$_1^4$-based data set. The first 2D NCA plane of the 3D PARS spectrum is shown in Figure 6(a); the resonance assignments were reported by us previously.[35] The corresponding ^{1}H-^{15}N dipolar line shapes for each residue were extracted along the third

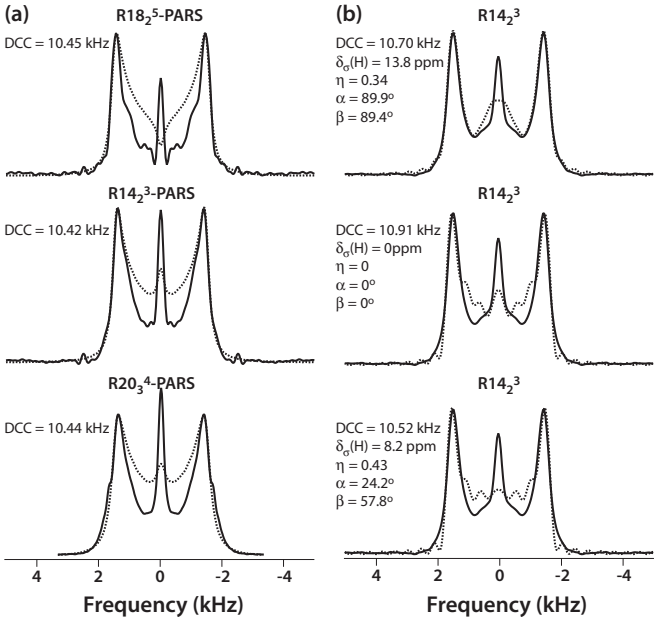

FIG. 5. Experimental (solid lines) and best-fit (dashed lines) ^{1}H-^{15}N dipolar line shapes of [^{15}N]- NAV recorded by (a) PARS and (b) conventional R-based sequences. The experiments were conducted at the magnetic field of 14.1 T and MAS frequency of 40 kHz. For the PARS experiments, the following RN symmetry sequences were employed: R18$_2^5$ with ^{1}H RF field of 180 kHz (top), R14$_2^3$ with ^{1}H RF field of 140 kHz (middle), and R20$_3^4$ with ^{1}H RF field of 133.3 kHz (bottom). (b) ^{1}H-^{15}N dipolar line shape obtained by conventional R14$_2^3$ recoupling sequence. The ^{15}N π pulses during PARS period were 7.0 μs wide and were applied with 8-step phase cycle. The spectrum was fitted to extract the dipolar coupling constant, using different fixed values of ^{1}H CSA parameters, shown next to each spectrum. Note the different resulting DCC values depending on the ^{1}H CSA used.

dimension in both 3D spectra, and we obtained a total of 53 PARS and 49 DIPSHIFT-RN dipolar patterns. We performed single fits of the conventional and PARS dipolar lineshapes, to extract the corresponding dipolar couplings; we did not include ^{1}H CSA into the fits. The resulting dipolar parameters are shown in Table S1 in the supplementary material.[49] Representative experimental and simulated ^{1}H-^{15}N dipolar line shapes for six LC8 residues are plotted in Figure 6(b). As is clear from Table S1 in the supplementary material[49] and Figure 6(b), there is considerable discrepancy between the DCC values extracted from the conventional R12$_1^4$ and the corresponding PARS spectra. Examples of conventional DIPSHIFT-RN/PARS determined DCCs are: 10.4/9.4 kHz (M13), 8.1/9.0 kHz (N51), and 9.3/9.1 kHz (Y65). These results highlight that in the conventional R-based experiments, the errors associated with the DCC values extracted from a single fit can vary significantly. Figure 7(a) shows the results of the detected residues in the form of order parameters, which are given by the ratio of the measured DCC and the DCC of a thermally static NH bond, assumed to be 11.34 kHz.[22] Even though for the majority of the residues the order parameters extracted from single fits of the conventional R12$_1^4$ spectra are overestimated, in some instances those can be underestimated, depending on the ^{1}H CSA parameters (see Figure 7(b)). We also note that in the conventional R12$_1^4$-based spectra of LC8, dipolar line shapes for several residues are missing, most likely due to the decay of ^{15}N T_2 relaxation

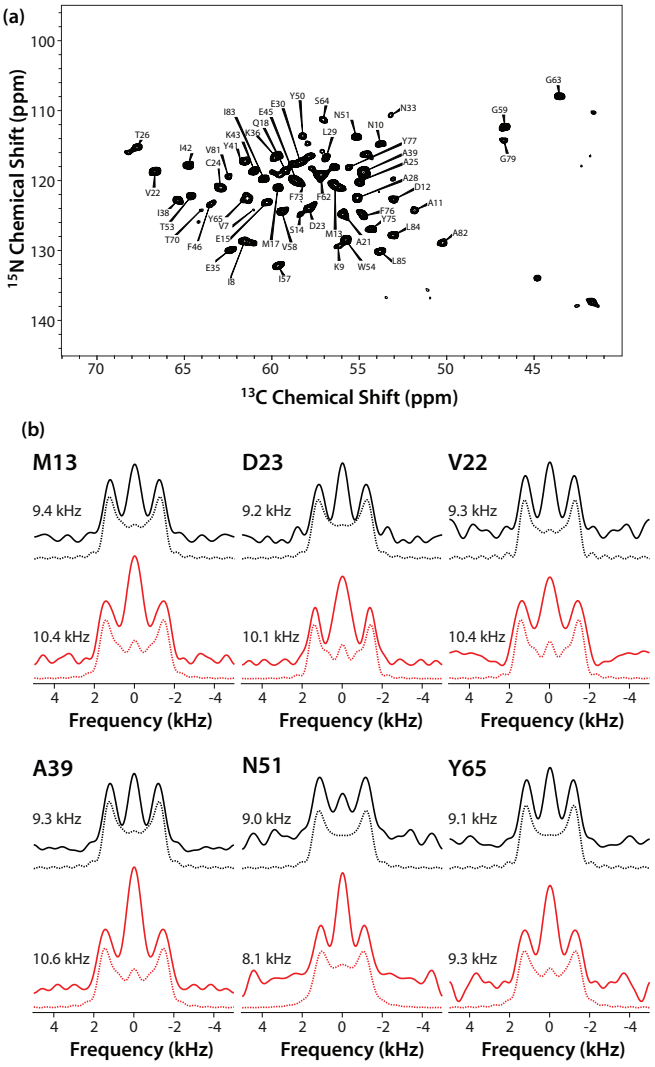

FIG. 6. (a) The 2D NCA plane (at $t_1 = 0$) of the 3D R12$_1^4$-based ^{1}H-^{15}N PARS spectrum of U-^{13}C,^{15}N-LC8. The spectrum was recorded at 19.97 T; the MAS frequency was 20 kHz. The ^{1}H RF field strength was 120 kHz for PARS recoupling. The ^{15}N π pulses during PARS period were 6.4 μs wide and were applied with 4-step phase cycle. (b) Representative experimental (solid lines) and simulated (dashed lines) ^{1}H-^{15}N dipolar line shapes for LC8 residues, extracted from the conventional R12$_1^4$ (red) and PARS R12$_1^4$ (black) spectra. ^{1}H CSA was not considered in fitting the spectra. The best-fit dipolar coupling constants are indicated next to each spectrum.

during the constant Hahn spin-echo period (see Figure 1(a)). In contrast, these line shapes were observed in the PARS spectra, which were recorded without constant echo time. Generally, PARS spectra exhibited higher sensitivity, particularly for the residues possessing short T_2 relaxation times.

The above ^{1}H-^{15}N dipolar coupling parameters contain information on the backbone motions occurring on the timescales of 10^{-6}–10^{-9} s. Figure 7(b) shows the differences between the ^{1}H-^{15}N dipolar order parameters obtained from PARS and conventional RN dipolar experiments. The average deviation in the dipolar order parameter is 0.091, with the largest discrepancy being 0.205 (for residue Y75). The average order parameters derived from DIPSHIFT-RN are 0.89 for the overall sequence, 0.91 for the secondary structure elements (α-helices and β-sheets), and 0.81 for loops. In comparison, the corresponding average order parameters derived

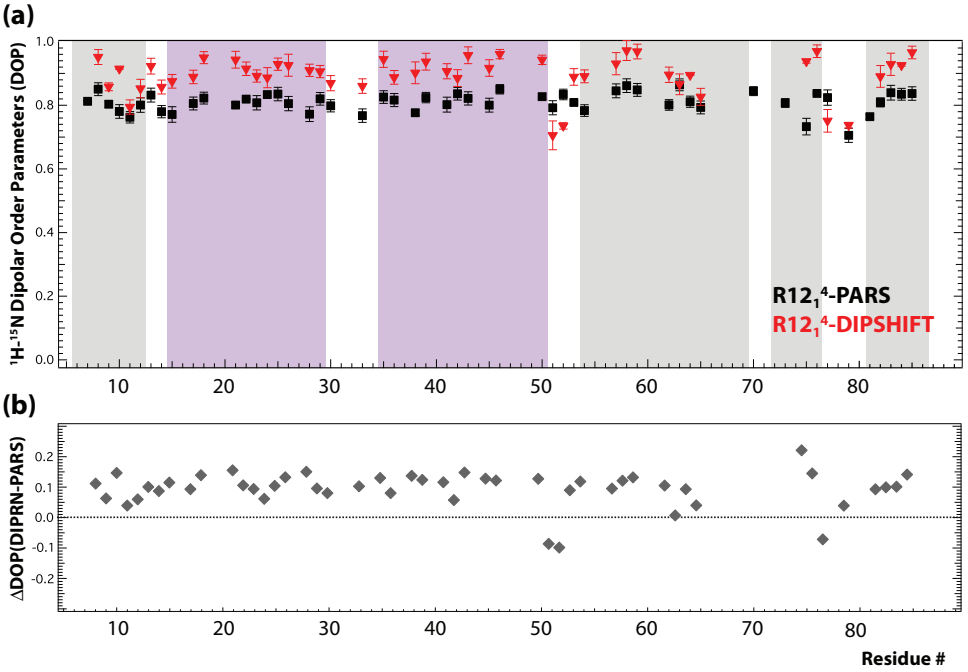

FIG. 7. (a) Overlay of ^{1}H-^{15}N dipolar order parameters (DOP) obtained experimentally for LC8 by R12$_1^4$-based PARS (black markers) and the conventional R12$_1^4$ dipolar recoupling (red markers) 3D sequences plotted versus the residue number. The DOPs were calculated using the rigid limit ^{1}H-^{15}N dipolar coupling constant of 11.34 kHz. The color coding of the plot corresponds to the LC8 secondary structure: grey (β-sheets), lavender (α-helices), and white (loops). (b) Differences in DOPs of LC8 extracted from R12$_1^4$-based PARS and conventional R12$_1^4$ dipolar recoupling plotted versus the residue number.

from PARS are 0.81, 0.81, and 0.79, and it can be seen that there is no much difference between the secondary structure elements and the loop regions, which suggests some backbone mobility throughout the entire protein, and the loop regions only exhibit slightly higher flexibility. This dynamic profile of LC8 is very different from profiles we have seen in other proteins and protein assemblies, such as thioredoxin[47] and CAP-Gly,[48] and HIV-1 CA protein assemblies (unpublished results) where loop regions exhibit much higher mobility on nano- to microsecond timescales as manifested in order parameters that are significantly lower than in the rigid secondary structure elements. It is also important to note that, despite the inaccuracies in the order parameters measured in a single conventional DIPSHIFT-RN experiment, which are of the order of 5%–12% at 19.9 T, the overall trends are correctly captured. Therefore, one can still use the conventional experiments for assessing qualitative trends in the mobility of different regions of protein, even for the measurements conducted at 17.6–21.1 T, as long as appropriate errors are attributed to such values that take into account the uncertainties due to ^{1}H CSA contributions.

CONCLUSIONS

In summary, the PARS sequences reported in this work establish a reliable method for the site-specific measurement of accurate heteronuclear dipolar couplings in organic and biological systems. The efficient suppression of ^{1}H chemical shift anisotropy contribution permits to extract accurate dipolar parameters in a single measurement and obviates the need for two additional experiments and simultaneous triple fitting of the data. The lack of sensitivity to recoupling pulse misset assures the robustness of the PARS recoupling. Finally, we have demonstrated that PARS performs efficiently under a wide range of MAS frequencies including fast MAS conditions. On the basis of the results we envision that PARS will be applicable to a wide variety of biological and organic systems.

ACKNOWLEDGMENTS

This work was supported by the National Institutes of Health (NIH Grant Nos. P50GM082251 and R01GM085306 and P30GM103519 from NIGMS) and is a contribution from the Pittsburgh Center for HIV Protein Interactions. We acknowledge the support of the National Science Foundation (NSF Grant No. CHE0959496) for the acquisition of the 850 MHz NMR spectrometer at the University of Delaware.

[1] J. Meiler, J. J. Prompers, W. Peti, C. Griesinger, and R. Bruschweiler, J. Am. Chem. Soc. **123**(25), 6098–6107 (2001).
[2] D. Huster, L. S. Xiao, and M. Hong, Biochemistry **40**(25), 7662–7674 (2001).
[3] R. Tycko, Prog. Nucl. Magn. Reson. Spectrosc. **42**(1–2), 53–68 (2003).
[4] D. S. Thiriot, A. A. Nevzorov, L. Zagyanskiy, C. H. Wu, and S. J. Opella, J. Mol. Biol. **341**(3), 869–879 (2004).
[5] W. T. Franks, D. H. Zhou, B. J. Wylie, B. G. Money, D. T. Graesser, H. L. Frericks, G. Sahota, and C. M. Rienstra, J. Am. Chem. Soc. **127**(35), 12291–12305 (2005).
[6] J. L. Lorieau and A. E. McDermott, J. Am. Chem. Soc. **128**(35), 11505–11512 (2006).
[7] A. McDermott and T. Polenova, Curr. Opin. Struct. Biol. **17**(5), 617–622 (2007).
[8] J. L. Lorieau, L. A. Day, and A. E. McDermott, Proc. Natl. Acad. Sci. U.S.A. **105**(30), 10366–10371 (2008).
[9] M. Sackewitz, H. A. Scheidt, G. Lodderstedt, A. Schierhorn, E. Schwarz, and D. Huster, J. Am. Chem. Soc. **130**(23), 7172 (2008).

[10]V. Chevelkov, U. Fink, and B. Reif, J. Am. Chem. Soc. **131**(39), 14018–14022 (2009).
[11]I. J. L. Byeon, G. J. Hou, Y. Han, C. L. Suiter, J. Ahn, J. Jung, C. H. Byeon, A. M. Gronenborn, and T. Polenova, J. Am. Chem. Soc. **134**(14), 6455–6466 (2012).
[12]B. J. van Rossum, C. P. de Groot, V. Ladizhansky, S. Vega, and H. J. M. de Groot, J. Am. Chem. Soc. **122**(14), 3465–3472 (2000).
[13]V. Ladizhansky and S. Vega, J. Chem. Phys. **112**(16), 7158–7168 (2000).
[14]M. Hohwy, C. P. Jaroniec, B. Reif, C. M. Rienstra, and R. G. Griffin, J. Am. Chem. Soc. **122**(13), 3218–3219 (2000).
[15]X. Zhao, M. Eden, and M. H. Levitt, Chem. Phys. Lett. **342**(3–4), 353–361 (2001).
[16]M. Bjerring and N. C. Nielsen, Chem. Phys. Lett. **370**(3–4), 496–503 (2003).
[17]M. Eden, Chem. Phys. Lett. **378**(1–2), 55–64 (2003).
[18]I. Schnell, Prog. Nucl. Magn. Reson. Spectrosc. **45**(1–2), 145–207 (2004).
[19]S. V. Dvinskikh, H. Zimmermann, A. Maliniak, and D. Sandstrom, J. Chem. Phys. **122**(4), 044512 (2005).
[20]F. Chou, S. Huang, and J. C. C. Chan, J. Magn. Reson. **197**(1), 96–99 (2009).
[21]P. Schanda, B. H. Meier, and M. Ernst, J. Am. Chem. Soc. **132**(45), 15957–15967 (2010).
[22]G. J. Hou, I. J. L. Byeon, J. Ahn, A. M. Gronenborn, and T. Polenova, J. Am. Chem. Soc. **133**(46), 18646–18655 (2011).
[23]P. Schanda, B. H. Meier, and M. Ernst, J. Magn. Reson. **210**(2), 246–259 (2011).
[24]M. F. Cobo, A. Achilles, D. Reichert, E. R. deAzevedo, and K. Saalwachter, J. Magn. Reson. **221**, 85–96 (2012).
[25]A. Gansmuller, J. P. Simorre, and S. Hediger, J. Magn. Reson. **234**, 154–164 (2013).
[26]P. Paluch, T. Pawlak, J. P. Amoureux, and M. J. Potrzebowski, J. Magn. Reson. **233**, 56–63 (2013).
[27]M. Carravetta, M. Eden, X. Zhao, A. Brinkmann, and M. H. Levitt, Chem. Phys. Lett. **321**(3–4), 205–215 (2000).
[28]A. Brinkmann and M. H. Levitt, J. Chem. Phys. **115**, 357–384 (2001).
[29]M. H. Levitt, in *Encyclopedia of Nuclear Magnetic Resonance*, edited by D. M. H. Grant and R. K. Harris (Wiley, Chichester, 2002), Vol. 9, pp. 165–196.
[30]R. K. Hester, J. L. Ackerman, B. L. Neff, and J. S. Waugh, Phys. Rev. Lett. **36**(18), 1081–1083 (1976).
[31]M. G. Munowitz, R. G. Griffin, G. Bodenhausen, and T. H. Huang, J. Am. Chem. Soc. **103**(10), 2529–2533 (1981).
[32]M. E. Stoll, A. J. Vega, and R. W. Vaughan, J. Chem. Phys. **65**(10), 4093–4098 (1976).
[33]G. J. Hou, S. Paramasivam, S. Yan, T. Polenova, and A. J. Vega, J. Am. Chem. Soc. **135**(4), 1358–1368 (2013).
[34]G. J. Hou, R. Gupta, T. Polenova, and A. J. Vega, Isr. J. Chem. **54**(1–2), 171–183 (2014).
[35]S. J. Sun, A. H. Butterworth, S. Paramasivam, S. Yan, C. M. Lightcap, J. C. Williams, and T. Polenova, Can. J. Chem. **89**(7), 909–918 (2011).
[36]B. M. Fung, A. K. Khitrin, and K. Ermolaev, J. Magn. Reson. **142**(1), 97–101 (2000).
[37]M. Bak, J. T. Rasmussen, and N. C. Nielsen, J. Magn. Reson. **147**(2), 296–330 (2000).
[38]M. Bak and N. C. Nielsen, J. Magn. Reson. **125**(1), 132–139 (1997).
[39]G. J. Hou, I. J. L. Byeon, J. Ahn, A. M. Gronenborn, and T. Polenova, J. Chem. Phys. **137**(13), 134201 (2012).
[40]M. Baldus, A. T. Petkova, J. Herzfeld, and R. G. Griffin, Mol. Phys. **95**(6), 1197–1207 (1998).
[41]N. Tjandra and A. Bax, J. Am. Chem. Soc. **119**(34), 8076–8082 (1997).
[42]M. Tessari, F. A. A. Mulder, R. Boelens, and G. W. Vuister, J. Magn. Reson. **127**(1), 128–133 (1997).
[43]G. Cornilescu and A. Bax, J. Am. Chem. Soc. **122**(41), 10143–10154 (2000).
[44]K. Loth, P. Pelupessy, and G. Bodenhausen, J. Am. Chem. Soc. **127**(16), 6062–6068 (2005).
[45]K. E. Kover, G. Batta, and V. J. Hruby, Magn. Reson. Chem. **41**(10), 828–836 (2003).
[46]L. S. Yao, A. Grishaev, G. Cornilescu, and A. Bax, J. Am. Chem. Soc. **132**(31), 10866–10875 (2010).
[47]J. Yang, M. L. Tasayco, and T. Polenova, J. Am. Chem. Soc. **130**(17), 5798–5807 (2008).
[48]S. Yan, "Microtubule-associated CAP-Gly domain of dynactin: structure, dynamics, conformational plasticity, and interactions with microtubules and microtubule plus-end tracking proteins by magic angle spinning NMR spectroscopy," Ph.D. dissertation (University of Delaware, Newark, DE, 2014).
[49]See supplementary material at http://dx.doi.org/10.1063/1.4894226 for supplementary figures, tables, and discussion on the influence of RF mismatch on experimental parameters.